JTTEE5 15:563-569
DOI: 10.1361/105996306X147252
1059-9630/$19.00 © ASM International

Simulation Results of Arc Behavior in Different Plasma Spray Torches

J.P. Trelles and J.V.R. Heberlein

(Submitted February 25, 2006; in revised form May 10, 2006)

Three-dimensional, transient simulations of the plasma flow inside different plasma spray torches have been performed using a local thermodynamic equilibrium model solved by a multiscale finite-element method. The model describes the dynamics of the arc without any further assumption on the reattachment process except for the use of an artificially high electrical conductivity near the electrodes. Simulations of an F4-MB torch from Sulzer-Metco and two configurations of the SG-100 torch from Praxair are presented. The simulations show that, when straight or swirl injection is used, the arc is dragged by the flow and then jumps to form a new attachment, preferably at the opposite side of the original attachment, as has been observed experimentally. Although the predicted reattachment frequencies are at present higher than the experimental ones, the model is suitable as a design tool.

Keywords arc dynamics, multiscale finite elements, plasma torch, time-dependent, three-dimensional

1. Introduction

Better reproducibility of plasma spraying processes is one of the major goals in current research and development efforts in thermal plasma technology (Ref 1). To achieve this goal, a better understanding of the dynamics of the arc inside direct current (dc) non-transferred arc plasma torches, as commonly used in plasma spraying, is required because the movement of the arc inside the torch has a first-order effect on both: coating quality (due to the forcing of the jet, enhancing cold flow entrainment and nonuniform powder heating) and anode lifetime (due to the localized heating of the anode).

Figure 1 shows schematically the flow inside a dc plasma torch. The arc dynamics are a result of the balance between the drag force caused by the interaction of the incoming gas flow over the arc and the electromagnetic (or Lorentz) force caused by the local curvature and thickness of the arc (Ref 2). The relative strength between these opposite forces leads to determination of three characteristic modes of operation of dc plasma torches (Ref 3-7): steady mode, characterized by slow or negligible movement of the arc; takeover mode, characterized by quasiperiodic movement; and restrike mode, characterized by chaotic movement with sudden and large voltage fluctuations.

The strong radiating nature of the arc, added to its confinement inside the torch, has prevented the direct observation of the complete arc dynamics. This has motivated the use of computational models to describe the behavior of the arc inside the torch. Modeling of the arc in dc plasma torches is very challenging because, despite the axisymmetry of the geometry and boundary conditions, the flow is inherently unsteady and three-dimensional; furthermore, the flow is highly nonlinear, with large gradients, and spans a wide range of time and spatial scales. In addition, chemical and thermodynamic nonequilibrium effects must be considered, especially near the boundaries of the plasma. The first simulations of the arc dynamics were performed by Baudry et al. (Ref 8, 9) using the code ESTET. They simulated the reattachment process by specifying a maximum electric field as control parameter and introducing an artificial hot column at a prespecified position upstream, simulating the formation of a new attachment. Recently, Colombo and Ghedini (Ref 10), using the commercial software FLUENT, simulated the plasma flow in a dc torch for a low current and flow rate. An adequate model should capture naturally, at least partially, the different modes of operation of the torch. Such a model has not yet been reported. In this paper, the authors present simulation results of a local thermodynamic equilibrium (LTE) model of the flow inside three different plasma torches. The model is capable of describing the steady and takeover modes of operation of the torch without any further assumption about the reattachment process except for the use of an artificially high electrical conductivity near the electrodes, which is needed because of the equilibrium assumption as done in Ref 11.

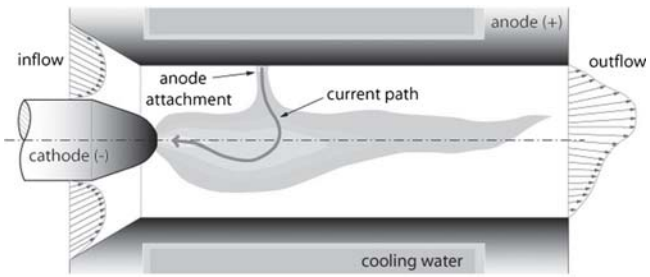

Fig. 1 Flow inside a dc non-transferred arc plasma torch

This article was originally published in *Building on 100 Years of Success: Proceedings of the 2006 International Thermal Spray Conference* (Seattle, WA), May 15-18, 2006, B.R. Marple, M.M. Hyland, Y.-Ch. Lau, R.S. Lima, and J. Voyer, Ed., ASM International, Materials Park, OH, 2006.

J.P. Trelles and **J.V.R. Heberlein,** Department of Mechanical Engineering, University of Minnesota, Minneapolis, Minnesota. Contact e-mail: jptrelles@me.umn.edu.

2. Mathematical Model

2.1 Model Assumptions

The continuum assumption is valid and the plasma is considered as a compressible, perfect gas in LTE, hence characterized by a single temperature T for all its species (atoms, ions, electrons, molecules); the quasineutrality condition holds; the plasma is optically thin; and Hall currents, gravitational effects, and viscous dissipation are considered negligible.

2.2 Governing Equations

Because the plasma is a conducting fluid, its description requires solution of the fluid conservation and electromagnetic equations, which, according to the assumptions stated above, are given by:

$$\frac{\partial \rho}{\partial t} + \nabla \cdot \rho \vec{u} = 0 \quad \text{(Eq 1)}$$

$$\rho\left(\frac{\partial \vec{u}}{\partial t} + \vec{u} \cdot \nabla \vec{u}\right) = -\nabla p - \nabla \cdot \overleftrightarrow{\tau} + \vec{j} \times \vec{B} \quad \text{(Eq 2)}$$

$$\rho C_p\left(\frac{\partial T}{\partial t} + \vec{u} \cdot \nabla T\right) = \nabla \cdot (\kappa \nabla T) + \vec{j} \cdot \vec{E}' - 4\pi\varepsilon_r + \frac{5}{2}\frac{k_B}{e}\vec{j} \cdot \nabla T - \left(\frac{\partial \ln \rho}{\partial \ln T}\right)_p \frac{Dp}{Dt} \quad \text{(Eq 3)}$$

$$\nabla \cdot (\sigma \nabla \phi) = 0 \quad \text{(Eq 4)}$$

$$\nabla^2 \vec{A} = -\mu_0 \vec{j} \quad \text{(Eq 5)}$$

where ρ is the fluid density, $\vec{u}$ velocity, p pressure, $\overleftrightarrow{\tau}$ the stress tensor; the term $\vec{j} \times \vec{B}$ represents the Lorentz force, with $\vec{j}$ as the current density and $\vec{B}$ the magnetic field; C_p is the specific heat at constant pressure, T temperature, κ thermal conductivity, and $\vec{j} \cdot \vec{E}'$ is the Joule heating term, with $\vec{E}'$ as the effective electric field ($\vec{E}' = \vec{E} + \vec{u} \times \vec{B}$); the term $4\pi\varepsilon_r$ represents the volumetric radiation losses with ε_r as the net emission coefficient; the term proportional to $\vec{j} \cdot \nabla T$ represents the diffusion of electron enthalpy, with k_B as Boltzmann's constant and e as the elementary charge; the last term in Eq 3 represents the pressure work (equal to zero in constant density flows), with D/Dt as the substantial derivative; σ is the electrical conductivity, ϕ the electric potential, $\vec{A}$ the magnetic vector potential, and μ_0 the permeability of free space. These equations are complemented with appropriate thermodynamic and transport properties and the following relations (with μ as the dynamic viscosity, and δ the identity tensor):

$$\overleftrightarrow{\tau} = -\mu\left(\nabla \vec{u} + \nabla \vec{u}^T - \frac{2}{3}\nabla \cdot \vec{u}\overleftrightarrow{\delta}\right) \quad \text{(Eq 6)}$$

$$\nabla \times \vec{A} = \vec{B}, \vec{E} = -\nabla\phi - \frac{\nabla \vec{A}}{\partial t}, \quad \text{and} \quad \vec{j} = \sigma \vec{E} \quad \text{(Eq 7)}$$

2.3 Computational Domain and Boundary Conditions

Figure 2 presents the computational domain of the torches studied, typically used in plasma spraying, as well as the computational mesh used for the simulations.

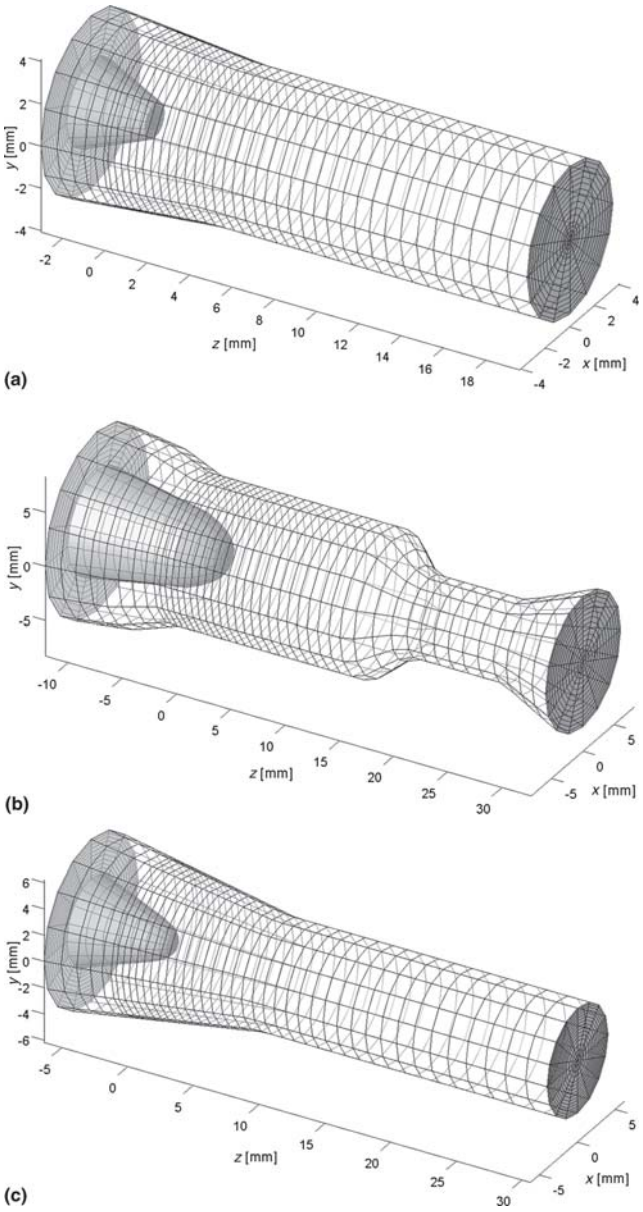

Fig. 2 Geometries studied: (a) torch 1, F4-MB torch from Sulzer-Metco; (b) torch 2 and (c) torch 3 SG-100 torches from Praxair with different cathode-anode configurations. Each plot has a different scale; the coordinate axis is centered on the cathode tip.

To allow the specification of boundary conditions, the boundary of each computational domain is divided in different sides (Fig. 1). Table 1 shows the boundary conditions used in the simulations, where p_0 represents a reference pressure, u_{in} the imposed velocity profile (fully developed flow through an annulus), T_{in} the imposed inlet temperature of 1000 K, T_c the cathode temperature defined by a Gaussian profile from 1000 to 3600 K at the tip, h_w the convective heat-transfer coefficient at the water-cooled anode surface equal to 10^5 W m^{-2} K^{-1}, T_w a reference cooling water temperature of 500 K, and j_c the imposed current density over the cathode. A value of σ equal to 8000 $(\Omega\ \text{m})^{-1}$ is imposed over the first layer of elements directly in front of the electrodes to allow passage of the electrical cur-

Table 1 Boundary conditions

	p	$\vec{u}$	T	ϕ	$\vec{A}$
Side 1: inlet	$p = p_0$	$\vec{u} = \vec{u}_{in}$	$T = T_{in}$	$\partial_n \phi = 0$	$A_i = 0$
Side 2: cathode	$\partial_n p = 0$	$u_i = 0$	$T = T_c$	$\partial_n \phi = 0$	$\partial_n A_i = 0$
Side 3: cathode tip	$\partial_n p = 0$	$u_i = 0$	$T = T_c$	$-\sigma \partial_n \phi = j_c$	$\partial_n A_i = 0$
Side 4: outlet	$\partial_n p = 0$	$u_{i,n} = 0$	$\partial_n T = 0$	$\partial_n \phi = 0$	$A_i = 0$
Side 5: anode	$\partial_n p = 0$	$u_i = 0$	$-\kappa \partial_n T = h_w (T - T_w)$	$\phi = 0$	$\partial_n A_i = 0$

Note: n = outer normal to the surface; $i = x, y,$ or z

rent. This layer of elements is ~0.1 mm thick and mimics the effect of the plasma sheath. Results obtained with a coarser mesh (sheath of ~0.2 mm) produced significantly larger reattachment frequencies, whereas results with a finer mesh (sheath of ~0.05 mm) basically reproduced the same results presented herein. However, the use of smaller sheath thickness—a result of the use of better spatial resolution—makes complicates solution convergence more difficult because of the sharper gradients near the anode. A more detailed description of the boundary conditions used is found in Ref 12.

3. Numerical Model

Due to the multiscale nature of thermal plasma flows, the equations describing our mathematical model are solved using a subgrid scale finite-element method (SGS-FEM), developed by Hughes et al (Ref 11) which separates the solution of a given field into a large-scale component (solved over the computational mesh) plus a small or subgrid scale component (modeled by the method). The SGS-FEM applied to nonlinear transient advective-diffusive-reactive systems has been implemented in the code HTPLFLOW (high temperature and plasma flow solver) developed in our laboratory. The code can solve an arbitrary number of equations in any number of spatial dimensions on unstructured grids in a fully implicit manner.

4. Simulation Results

Table 2 presents the operating conditions of the cases presented here; they were selected to allow direct comparison of the effects associated with torch geometry.

4.1 Torch 1

This geometry has been studied by Baudry et al. (Ref 8, 9). They performed simulations using the same current and flow rate used here, but using swirl instead of straight injection.

Figure 3 shows a time sequence of the temperature distribution through the vertical plane of the reattachment process. Because straight injection is used, the arc movement is expected to remain constrained in the vertical plane (y-z plane, Fig. 2). As can be seen, the arc is initially dragged by the incoming flow; as the flow pushes the arc downstream, the curvature of the arc increases, which increases the magnetic forces on the arc and pushes the arc to form a new attachment at the opposite side in the y direction of the original attachment. Once a new attachment is formed, the arc first moves upstream until the drag of the incoming flow pushes it downstream again, which starts a new

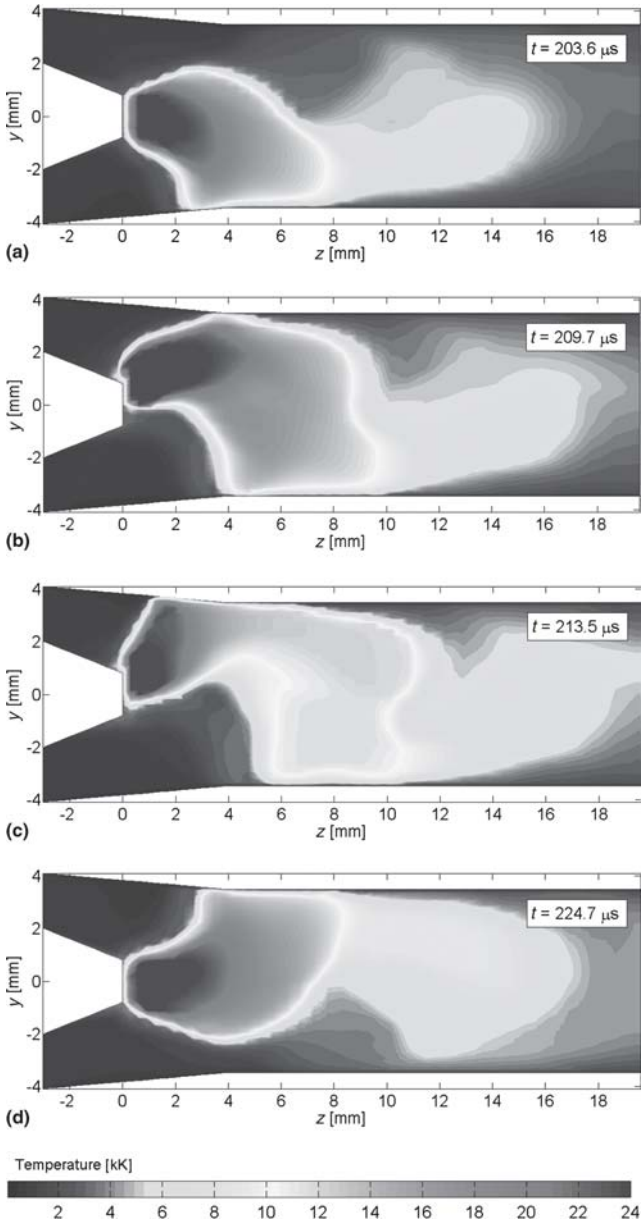

Fig. 3 Reattachment process in torch 1 (T, vertical plane)

Table 2 Operating conditions for the studied cases

	Gas	Current, A	Flow rate, slpm	Injection
Torch 1	Ar-H_2	600	60	Straight
Torch 2	Ar-H_2	600	60	Straight
Torch 3a	Ar-H_2	600	60	Straight
Torch 3b	Ar-H_2	600	60	Swirl

reattachment cycle. This arc behavior was also studied in previous simulations and is explained with greater detail in Ref 12.

4.2 Torch 2

The geometry of torch 2 is significantly different from torch 1 as it presents a sudden constriction of the anode, a much larger diameter, and a larger and more rounded cathode tip.

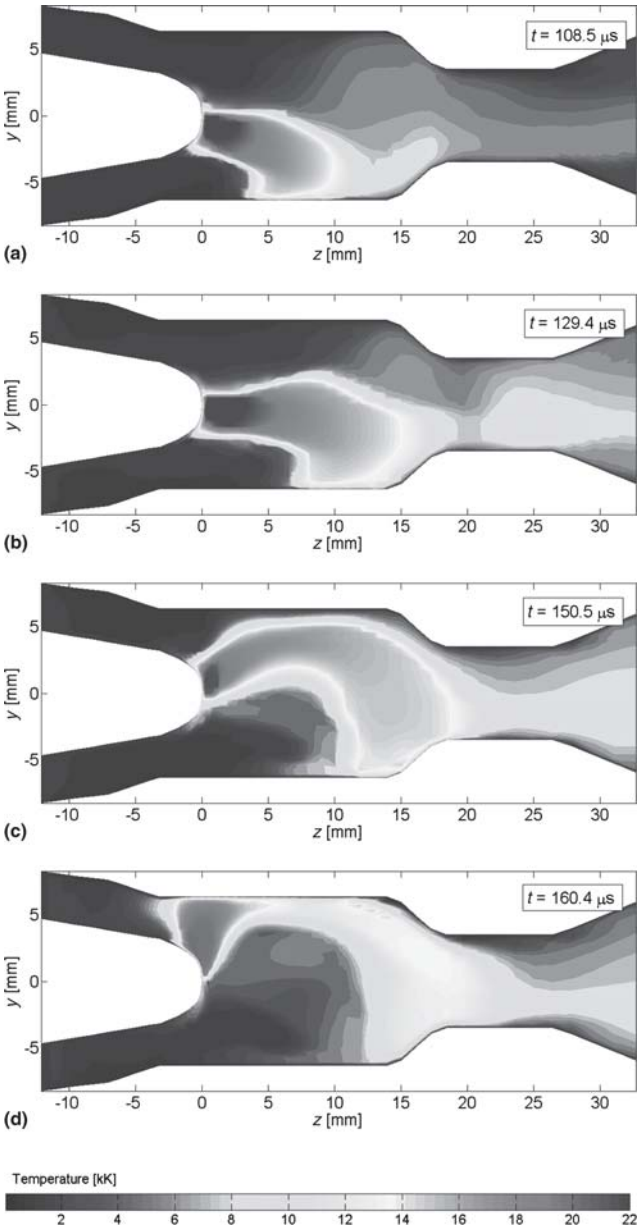

Fig. 4 Reattachment process in torch 2 (T, vertical plane)

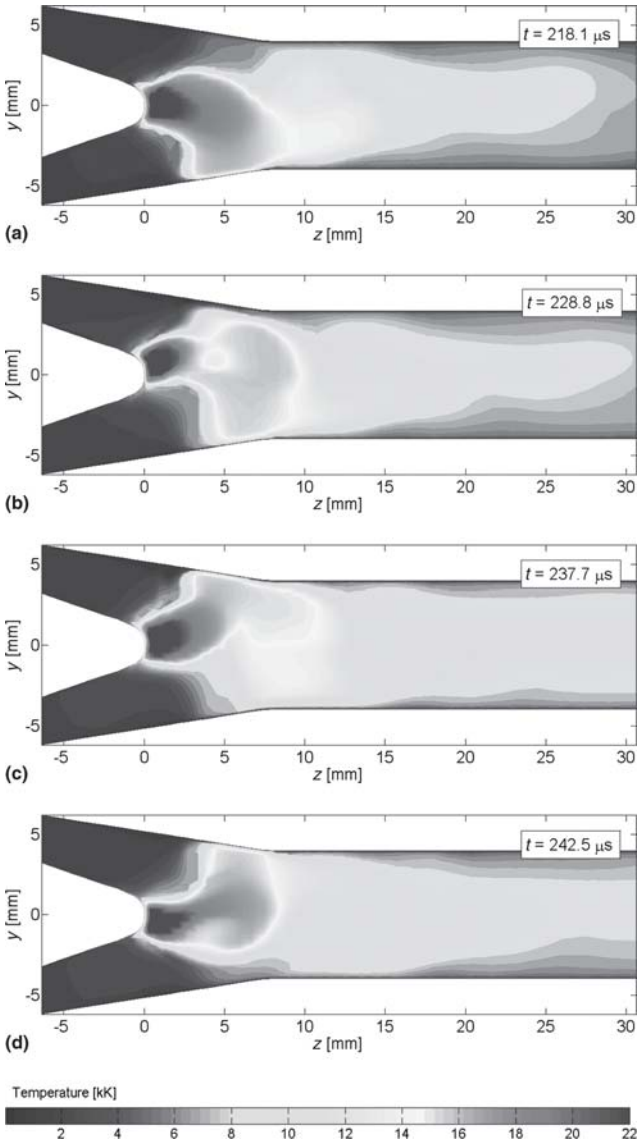

Fig. 5 Reattachment process in torch 3a (T, vertical plane)

Figure 4 shows a time sequence of the reattachment process for this torch. It is observed that the constriction of the anode downstream limits axial movement of the arc. The highest temperatures are observed when the arc is centered on the torch axis.

4.3 Torch 3

Figure 5 shows a time sequence of the reattachment process for torch 3a. Because of the figure's scale, the arc seems shorter than for torch 1; however, it is actually longer (the position of the anode attachment is at ~5 mm downstream from the cathode tip, whereas for torch 1 this distance is ~4 mm). It can also be observed that the arc in this geometry is less robust than that in torch 1. These characteristics are results of the weaker acceleration experienced by the flow as it enters the region downstream of the cathode, which has a larger diameter than its counterpart in torch 1 (8 versus 7 mm).

In Fig. 6 can be observed the temperature distribution inside the torch when swirl injection is used (torch 3b); the three-dimensionality of the flow is clearly observed. From these results, it is clear that the arc cannot be described adequately by a two-dimensional or a steady-state model.

This three-dimensionality does not allow us to present a reattachment sequence for torch 3b in plots similar to the previous figures. The reattachment process is shown sequentially in Fig. 7: between the top and center figures, the anode attachment is dragged axially and circumferentially counterclockwise with respect to the *z* axis, as if tracing a helix. In the center figure, the beginning of the formation of a new attachment can be observed at almost the opposite side of the original attachment. This new attachment becomes dominant, completing the reattachment

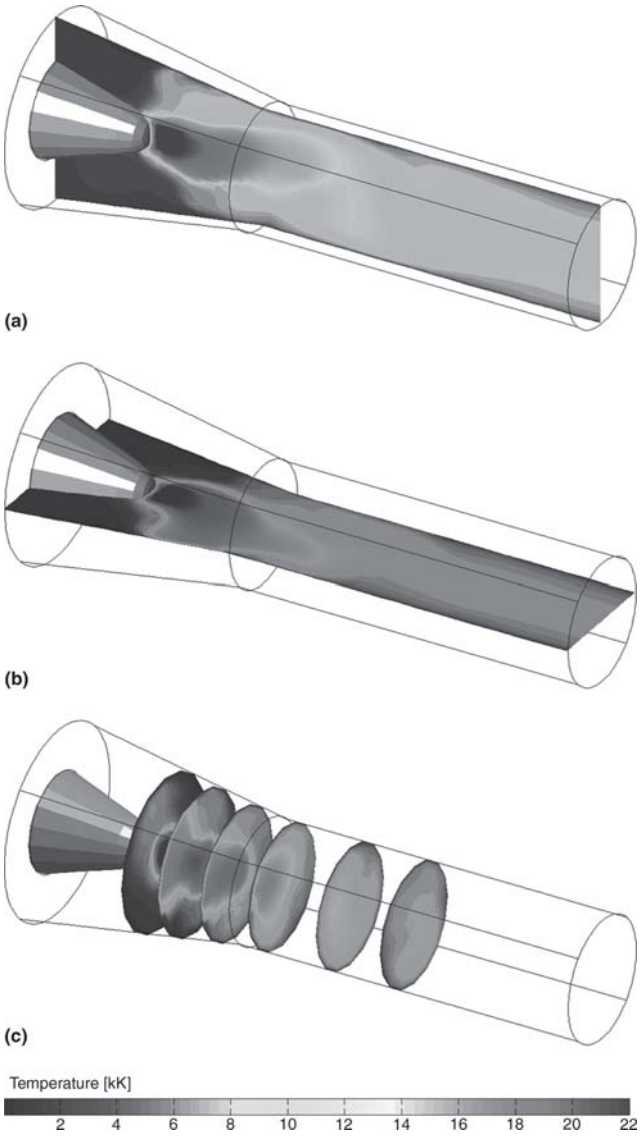

Fig. 6 Temperature distribution through vertical, horizontal, and axially distributed cross sections for torch 3b

process and leaving the arc in the position shown in the bottom figure, thus completing a reattachment cycle. The new arc then starts being dragged by the flow, and a new cycle is initiated.

This behavior of the arc is explained as follows. As the arc is dragged around the anode surface, it lengthens, its curvature increases, which produces an increase of the magnetic forces acting on it, pushing the arc to the opposite side of the attachment and leading to the formation of a new attachment, almost at the opposite side of the original one. This behavior has been observed experimentally in our laboratory by the use of end-on imaging of the arc and has been reported in Ref 4.

4.4 Time-Dependent Characteristics and Frequency Analysis

Because the voltage drop is proportional to the arc length, the movement of the arc is reflected by the voltage drop signal,

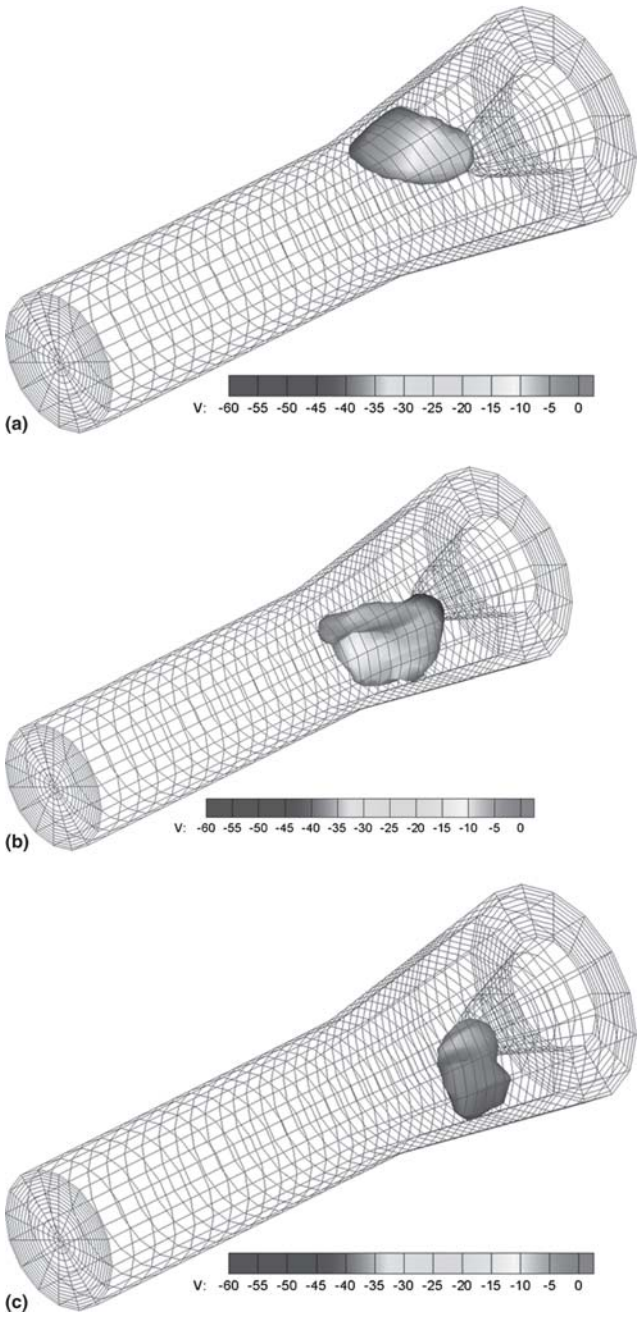

Fig. 7 Time sequence of reattachment process for torch 3b; electric potential distribution over the 14,000 K isosurface (representing the shape of the arc)

which is strongly correlated to other characteristics of the flow inside the torch, such as maximum and average temperatures, velocities, and pressure drops. Voltage traces of the cases simulated as well as experimental results from Ref 14 are presented in Fig. 8, where the rectangle in the bottom figure indicates the approximate time scale of the simulation results shown. While the conditions of the experiment in Ref 14 (SG-100 torch, 700 A, Ar 63 slpm, H2 5 slpm) do not exactly match the conditions in the authors' simulations, they are sufficiently close to the simulation conditions for torch 3b to allow a comparison. As expected, the greater percentage of H_2 used in torch

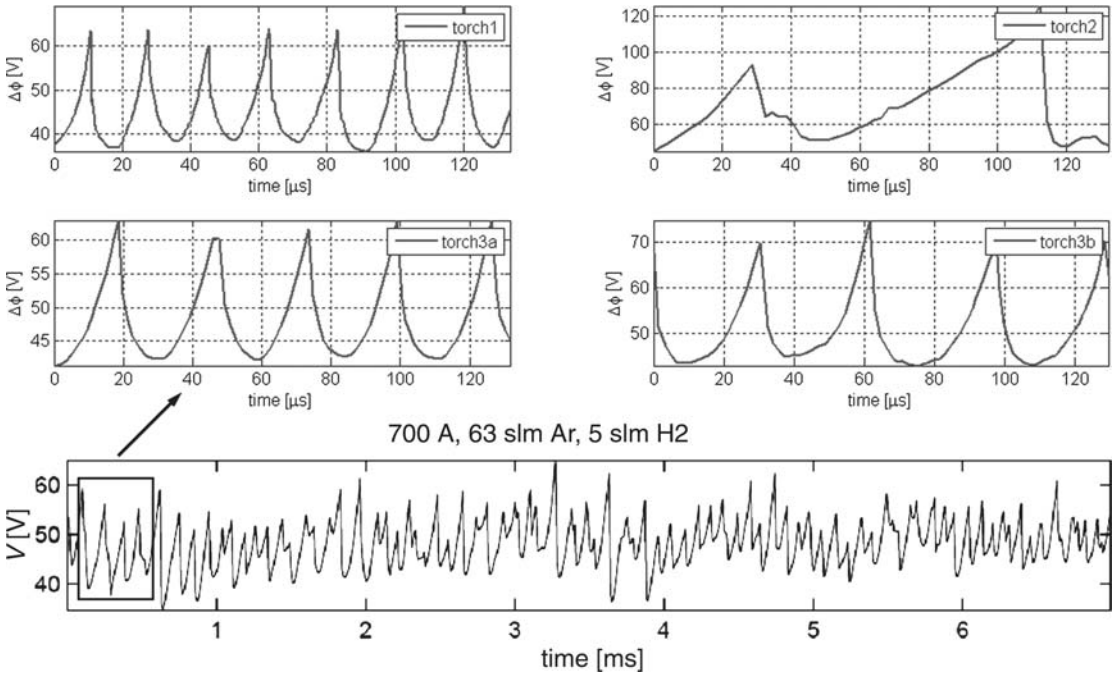

Fig. 8 Voltage traces for the torches simulated and experimental voltage trace reported in Ref 14

3b causes a larger reattachment frequency and a larger voltage drop. Bauldry's simulations have been used as basis for the cases studied here. The authors are currently in the process of comparing their results with experimental data. The frequency analysis of the total voltage drop over time obtained from our simulations allows the main reattachment periods and frequencies of the plasma flow to be determined. These characteristics allow more direct comparison with experimental measurements because analysis of the voltage signal is commonly used as a parameter for determination of arc characteristics under the given operating conditions. Table 3 summarizes the reattachment periods and frequencies as well as axial velocity averaged over time and radius and temperature at the outlet obtained from our simulations. The effect of the anode diameter can be clearly deduced from this table: as the diameter is increased, the reattachment frequency is decreased. Furthermore, the effect of the constriction of the anode in torch 2 evidences the lengthening of the reattachment period. So far, the frequencies obtained in the simulations are typically a factor of 2-4 larger than those obtained experimentally. Moreover, the obtained velocities and temperatures at the outlet are 30-40% smaller than the measured values. We expect that the use of better spatial resolution in our simulations as well as the use of a nonequilibrium model will allow better agreement with experiments.

Table 3 Predicted reattachment periods, frequencies, time averaged mean velocity, and temperature at the outlet

	Reattachment period, μs	Reattachment frequency, kHz	Mean velocity at outlet, m/s	Mean temperature at outlet, K
Torch 1	48.3	20.7	498	5240
Torch 2	85.2	11.7	547	4460
Torch 3a	19.7	50.7	345	4087
Torch 3b	27.0	37.0	317	4023

5. Conclusions

Three-dimensional, transient simulations of three different torch geometries have been performed to study the behavior of the arc inside plasma-spraying torches. It has been observed that, when swirl or straight injection is used, the arc will initially be dragged by the incoming flow and will then reattach, preferably at the opposite side of its original attachment. This phenomenon, observed experimentally, seems to be caused primarily by the imbalance between drag and electromagnetic forces. Although the reattachment frequencies obtained by our model are presently a factor of 2-4 larger than the experimental frequencies, the model can be used as a tool for the design of plasma-spraying torches.

Acknowledgments

This research has been supported by the NSF (grant CTS-0225962). Computing time from a grant from the University of Minnesota Supercomputing Institute (MSI) is gratefully acknowledged. The authors especially thank Shuxia Zhang from the MSI for her help in the implementation of our code.

References

1. E. Pfender, Thermal Plasma Technology: Where Do We Stand and Where Are We Going, *Plasma Chem. Plasma Process.,* 1999, **19**(1), p 1-31
2. S.A. Wutzke, "Conditions Governing the Symptomatic Behavior of an Electric Arc in a Superimposed Flow Field," Ph.D. thesis, University of Minnesota, 1967

3. Z. Duan, J. Heberlein, S. Janisson, K. Wittmann, J.F. Coudert, and P. Fauchais, Effects of Nozzle Fluid Dynamics on the Dynamic Characteristics of a Plasma Spray Torch, *United Thermal Spray Conf., Tagungsband,* E. Lugscheider and P.A. Kammer, Ed., ASM Thermal Spray Society 1999, p 247-252
4. Z. Duan, "Investigations of Plasma Instabilities in a Spray Torch," Ph.D. thesis, University of Minnesota, 2000
5. Z. Duan and J.V.R. Heberlein, Arc Instabilities in a Plasma Spray Torch, *J. Therm. Spray. Technol.,* 2002, **11**(1), p 44-51
6. J.F. Coudert and P. Fauchais, Arc Instabilities in a DC Plasma Torch, *High Temp. Mater. Process.,* 1997, **1,** p 149-166
7. J.F. Coudert, M.P. Planche, and P. Fauchais, Characterization of DC Plasma Torch Voltage Fluctuations, *Plasma Chem. Plasma Process.,* 1996, **16**(1), p 211S-227S
8. C. Baudry, A. Vardelle, and G. Mariaux, Numerical Modeling of a DC Non-Transferred Plasma Torch: Movement of the Arc Anode Attachment and Resulting Anode Erosion, *High Temp. Mat. Proc.,* 2005, **9**, p 1-15
9. C. Baudry, "Contribution à la Modélisation Instationnaire et Tridimensionnelle du Comportement Dynamique de l'Arc Dans une Torche de Projection Plasma," Ph.D. thesis, Universitè de Limoges, 2003
10. V. Colombo and E. Ghedini, Time-Dependent 3-D Simulation of a DC Non-Transferred Arc Plasma Torch: Anode Attachment and Downstream Region Effects, *Proc. 17th Int. Symp. Plasma Chemistry,* (Toronto, CA), 2005, p 169
11. H.-P. Li, E. Pfender, and X. Chen, Application of Steenbeck's Minimum Principle for Three-Dimensional Modelling of DC Arc Plasma Torches, *J. Phys. D, Appl. Phys.,* 2003, **36,** p 1084-1096
12. J.P. Trelles, E. Pfender, and J.V.R. Heberlein, Multiscale Finite Element Modeling of Arc Dynamics in a DC Plasma Torch, *Plasma Chem. Plasma Process.,* 2006, in press. Available at http://www.springerlink.com/content/1572-8986/?sortorder=asc&content+status=accepted
13. T.J.R. Hughes, G.R. Feijoo, L. Mazei, and J.B. Quincy, The Variational Multiscale Method: A Paradigm for Computational Mechanics, *Comput. Methods Appl. Mech. Eng.,* 1998, **166,** p 3-24
14. M. Vysohlid and J. Heberlein, Investigation of Arc Voltage Fluctuations in a Plasma Torch SG-100 Operated with Ar/H_2, *Thermal Spray 2004: Advances in Technology and Application,* May 10-12, 2004 (Osaka, Japan), ASM International, 2004